

Interactions between dislocations and irradiation-induced defects in light water reactor pressure vessel steels

Stéphanie Jumel^{a,b,*}, Jean-Claude Van Duysen^{a,b},
Jacky Ruste^a, Christophe Domain^{a,b}

^a *Électricité de France, Division Recherche et Développement, Site des Renardières, 77818 Moret sur Loing, France*

^b *Laboratoire de Physique et Génie des Matériaux (LMPGM), Université des Sciences et Technologies de Lille I, 59655 Villeneuve d'Ascq, France*

Received 8 February 2005; accepted 20 April 2005

Abstract

The REVE project (REactor for Virtual Experiments) is an international effort aimed at developing tools to simulate irradiation effects in light water reactors materials. In the framework of this project, a European team developed a first tool, called RPV-1 designed for reactor pressure vessel steels. This article is the third of a series dedicated to the presentation of the codes and models used to build RPV-1. It describes the simplified approach adopted to simulate the irradiation-induced hardening. This approach relies on a characterization of the interactions between a screw dislocation and irradiation-induced defects from molecular dynamics simulations. The pinning forces exerted by the defects on the dislocation were estimated from the obtained results and some hypotheses. In RPV-1, these forces are used as input parameters of a Foreman and Makin-type code, called DUPAIR, to simulate the irradiation-induced hardening at 20 °C. The relevance of the proposed approach was validated by the comparison with experimental results. However, this work has to be considered as an initial step to facilitate the development of a first tool to simulate irradiation effects. It can be improved by many ways (e.g. by use of dislocation dynamics code).

© 2005 Elsevier B.V. All rights reserved.

1. Introduction

Many key components in commercial nuclear reactors are subject to neutron irradiation which modifies their mechanical properties. So far, the prediction of

the in-service behavior and the lifetime of these components have required to irradiate materials in so-called 'Experimental Test Reactors'. For example, large-scale irradiation programs have been carried out in many countries to assess the end-of-life behavior of pressure vessel or internal structures of light water reactors (LWRs), or to develop cladding materials for fuel elements. This predominantly empirical approach does not cover all the needs, mainly because some in-service conditions are almost impossible to reproduce with the existing test facilities. Moreover, experimental programs

* Corresponding author. Address: European Institute for Energy Research, Universität Karlsruhe, Emmy-Noether-Str. 11, 76131 Karlsruhe, Germany.

E-mail address: stephanie.jumel@edf.fr (S. Jumel).

are becoming more problematic due to the decreasing number of test reactors and post-irradiation characterization facilities. Their increasing cost is also a serious drawback.

A proactive way to meet these issues is to develop physically based computer tools to numerically simulate irradiation effects. The development of such tools (we call them Virtual Test Reactors or VTRs) is now accessible thanks to continuous progress in physical understanding of material degradation as well as in computer science and technology. It can take advantage of the large and burgeoning field of computational material sciences. However, specific suites of multi-scale simulation codes have to be constructed by the irradiation effects community (e.g. [1,2]).

The devising of VTRs started in the framework of the REVE Project (REactor for Virtual Experiments). This project (e.g. [3–5]) is a joint effort between Europe, the United States and Japan aimed at building VTRs able to simulate irradiation effects in pressure vessel steels and internal structures of LWRs. In this framework, the European team has already built a first VTR, called RPV-1, designed for reactor pressure vessel steels (RPV steels) [5]. Some of the codes and data it uses, have been provided by the US and Japanese teams (led respectively by Prof. R. Odette from the University of California Santa Barbara and Dr N. Soneda from Central Research Institute of Electric Power Industry).

RPV-1 relies on many simplifications and approximations and has to be considered as a prototype developed to clear the way. Long-term efforts will be required to complete it and to build successive generations of more and more sophisticated versions. Nevertheless, RPV-1 can already be used for many applications (e.g. understanding of experimental results or assessment of material and irradiation conditions effects). Its input and output data are similar to those of experimental irradiation programs carried out to assess the in-service behavior of reactor pressure vessels.

This article is the third of a series aimed at presenting the codes and models used to build RPV-1 [6,7]. It describes the simplified approach followed to simulate the irradiation-induced hardening at 20 °C. This approach can be improved by many obvious ways, but it must be emphasized that the required effort is beyond the scope of the work carried out to build RPV-1. The main objective of this work was to build a reasonable first demonstration tool and not a perfect tool.

2. Irradiation-induced hardening of RPV steels

This paragraph is aimed at summarizing the knowledge on irradiation-induced defects in RPV steels and on their interaction with dislocations. Presented results will be used in Section 5 to approximate the pinning forces exerted by the defects on a screw dislocation.

2.1. Irradiation-induced defects

It is well established that the irradiation-induced hardening of RPV steels derives from the formation of a high number density of nanometer-sized defects. At least four types of defects have been identified. In spite of some controversies, the current knowledge about the microstructure and hardening effect can be described in the following way (e.g. [8,9]).

Copper-rich precipitates: these defects have a radius lower than about 1.5 nm and a number density of some 10^{24} m^{-3} , for a fluence of some $10^{19} \text{ n cm}^{-2}$ ($E \geq 1 \text{ MeV}$) and an irradiation temperature of about 290 °C (e.g. [10]); they contain Mn, Ni, Si and probably Fe. Tomographic Atom Probe experiments [11] carried out on binary alloys (Fe–0.7%Cu, Fe–1.4%Cu) irradiated with electrons or neutrons at 288 °C gave a rather precise description of the morphology of irradiation-induced ‘pure’ copper precipitates in iron at this temperature (Fig. 1). Such precipitates can be described as a core zone,

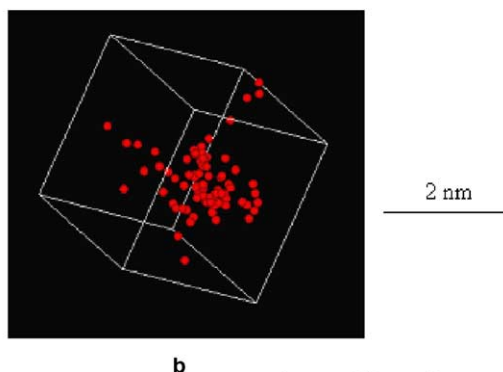
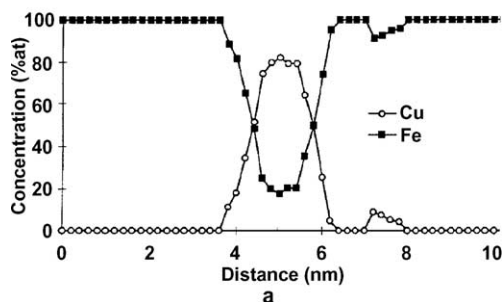


Fig. 1. Tomographic atom probe results [11]. (a) Concentration profile through a copper precipitates induced by neutron irradiation in a Fe–1.4%Cu. (b) Cluster of copper atoms observed in an Fe–0.1%Cu alloys irradiated with neutron at 288 °C.

with a diameter of about 1 nm, containing about 80% of copper (thus 20% of iron) and surrounded by a diffuse interface with the matrix. Irradiation-induced copper-rich precipitates in RPV steels are thought to have a similar structure. There are some experimental (e.g. [11]) or modeling [10] evidences showing the Ni, Mn and Si mainly concentrate at their interface with the matrix.

In first studies, copper-rich precipitates were described as ‘soft’ spots that attract dislocations by lowering their elastic energy. The phenomenon was assumed to arise from the difference between their shear modulus and that of the surrounding matrix (e.g. [12,13]) and was assessed in terms of the Russell and Brown model [14]. Another explanation based on non-elastic effect within the dislocation core was put forward by Phythian et al. [13] and then by Harry and Bacon [15]. From molecular dynamics (MD) simulations, they noticed that a dislocation may transform the bcc structure of copper precipitates embedded in α -iron into a new one having similarities with a fcc structure. More precisely, Harry and Bacon reported that the dislocation core of a screw dislocation spreads in the precipitate and transforms its structure, leading to a lower energy configuration. The larger the precipitate, the more its structure moves to fcc. In both models, copper-rich precipitates are expected to pin the dislocation and the strengthening effect results from the difficulty to pull the dislocation out of them. The role played by Mn, Ni and Si atoms in the strengthening has not been the object of dedicated studies yet. However, it was suggested that Mn and Ni could strongly contribute by forming an ordered structure [10].

Vacancy clusters: these defects have a radius lower than about 0.5 nm and number density of some 10^{24} m^{-3} , for a fluence of some $10^{19} \text{ n cm}^{-2}$ ($E \geq 1 \text{ MeV}$) and an irradiation temperature of about $290 \text{ }^\circ\text{C}$ (e.g. [10,16]). They pin the dislocations through a mechanism initially analyzed by Coulomb and Friedel [17]. These authors considered that if the radius (r) of the cavity is much larger than the core radius of the dislocation, the binding energy (E_{Bind}) between the two defects can be approximated by the energy corresponding to the missing segment of dislocation line: $E_{\text{Bind}} = 2rE_{\text{Line}}$, where E_{Line} is the energy of the dislocation line per length unit ($E_{\text{Line}} \approx \frac{\mu b^2}{2}$ where μ is the shear modulus and b , the Burgers vector); Osetsyky and Bacon [18] recently confirmed this result by molecular dynamics simulations for an edge dislocation.

A more precise elastic calculation by Bullough and Newman [19] showed that the long-range elastic interaction between a cavity and a screw dislocation is given by $E_{\text{Inter}} = \frac{-5\mu b^2 r^2 (1-\nu)}{2\pi(7-5\nu)d^2}$ where d is the distance between both defects and ν , the Poisson’s ratio. For a dislocation tangential to the cavity, they approximated the interaction energy by using this expression with $d = r$ (which leads to $E_{\text{Inter}} \approx \mu b^2/10$). They also estimated that the pin-

ning force is at most $\mu b^2/5$ (when the slip plane is through the center of the cavity) and on average $\mu b^2/10$ ($\approx 3 \text{ eV/nm}$).

Vacancy–solute atom (Cu, Mn, Ni, Si) clusters: experimental characterizations (atom probe, small angle neutron scattering) revealed the presence of solute atom clusters in irradiated RPV steels. These defects have a radius lower than about 1.5 nm and a number density of some 10^{24} m^{-3} , for a fluence of some $10^{19} \text{ n cm}^{-2}$ ($E \geq 1 \text{ MeV}$) and an irradiation temperature of about $290 \text{ }^\circ\text{C}$ (e.g. [20]). They contain Cu, Mn, Ni, Si atoms and a high concentration of Fe atoms (about 85%) which gives them a dilute aspect (they are often called ‘atmospheres’ or ‘clouds’ of solute atoms). This aspect was clearly shown by atom probe characterizations on neutron-irradiated binary Fe–Cu alloys (Fig. 1(b)) [11]. The reason why these defects keep a dilute morphology and do not collapse in a real precipitate is an issue still under discussion. One possible explanation could be the presence of vacancies within the defects. This explanation is at the origin of their name: vacancy–solute atom clusters. Molecular dynamics simulations suggest that such clusters could be made of small vacancy–copper atom complexes (some vacancies and copper atoms linked together) ‘turning around each other’, merging and splitting in a volume of some cubic nanometers. It is maybe the iron atoms of this volume which are revealed in the defects by the atom probe.

To our knowledge, no model has been developed to explain the strengthening effect of vacancy–solute atom clusters. It can be assumed that they pin the dislocation by a mix of several contributions, depending on the copper and vacancy contents: vacancy cluster-type, copper precipitate-type or solid solution-type strengthening.

Self-interstitial-atom clusters (SIA-clusters): these defects have a radius lower than 2 nm and a number density of some 10^{24} m^{-3} , for a fluence of some $10^{19} \text{ n cm}^{-2}$ ($E \geq 1 \text{ MeV}$) and an irradiation temperature of about $290 \text{ }^\circ\text{C}$. Their structure is not fully understood yet. In particular, the set of properties that distinguishes SIA-clusters and well defined SIA dislocation loops is not well clarified [21–24]. According to Puigvi et al. [21] and Kuramoto [23], between about 160 and 200 SIAs are required for a cluster to fully behave as a dislocation loop; except at a very small size. Wirth et al. (e.g. [22]) reckon that both types of defect have analogous properties and can be considered as similar. For the building of RPV-1, we retained this position and considered that the SIA clusters behave as dislocation loops, whatever their size [7].

TEM examinations of ferritic alloys irradiated with high doses ($\geq 1 \text{ dpa}$) (e.g. [25,26]) as well as MD simulations in Fe (e.g. [22,27–29]) showed that the stable SIA loops have for Burgers vector $b = \frac{1}{2}\langle 111 \rangle$ or $\langle 100 \rangle$. Wirth et al. [22] described the $\frac{1}{2}\langle 111 \rangle$ loops as a mixture

of $\langle 111 \rangle$ dumbbells and crowdions on $\{110\}$ planes, Soneda and Diaz de La Rubia [27] and Osetsky et al. [28] saw the crowdions only. Osetsky described the $\langle 100 \rangle$ loops as a set of $\langle 100 \rangle$ crowdions.

The interactions between a dislocation loop and a glissile dislocation can be classified in two types, ‘elastic’-type and ‘reaction’-type.

Elastic interaction: the elastic interaction between a prismatic loop and a dislocation has been calculated by several authors (e.g. [30–34]) in the approximation of isotropic elasticity. According to this approximation, there is no elastic interaction between a loop and a screw dislocation with a line perpendicular to the loop habit plane when the two Burgers vectors are parallel (e.g. [32]). Kroupa [30] calculated the elastic interaction when the two Burgers vectors are not parallel. He showed that the dislocation can be attracted or repelled by the loop according to the relative position of both defects.

Reaction interaction: when the loop and the dislocation intersect, they may combine and form a junction which can pin the dislocation (e.g. [35]). Friedel estimated that a junction led to a pinning force $F_{\max} \approx \frac{\mu b^2}{4}$ [36], Kimura and Maddin proposed a value of $\frac{\mu b^2}{8}$ [37]. The junction may be unstable and evolve, which transforms the loop: Foreman and Sharp [38] (generalizing a model proposed by Saada and Washburn [35]) described a mechanism where the loop combines with the dislocation to form a segment of the gliding dislocation (Fig. 2(a)). Hirsch [39] proposed another mechanism where the junction evolves to form a helix on the dislocation (Fig. 2(b)). Both mechanisms provide an explanation on the way gliding dislocations can sweep out loops and form cleared channels in iron-based alloys (e.g. [40]).

2.2. Thermal activation

At temperature above 0 K, dislocations can overcome irradiation-induced defects with the assistance of thermal energy. This thermal effect may result from a modification of the interaction mechanism between both types of defects or from the atomic fluctuations.

Modification of the interaction: thermal energy can weaken the interaction between dislocations and defects. Bacon and Osetsky [41] observed by MD simulations that the resolved shear stress required by an edge dislocation to overcome pure copper precipitates (100% Cu) and vacancy clusters decreases with increasing temperature. This effect has been attributed to a stronger tendency of dislocation climbing and weaker tendency for bcc-to-fcc transformation in the precipitates (see Section 2.1), as the temperature increases. It diminishes with decreasing size of the precipitates.

Atomic fluctuations: as the temperature increases, the atomic fluctuations increase and may help dislocations to overcome small defects. Such processes are characterized by a decreasing yield stress with increasing temperature up to a critical temperature (T_c) above which thermal fluctuations become so large that defects are overcome only by thermal energy. T_c is strain-rate-dependent and can be assessed from the following expression in the case of attractive obstacles [36]:

$$kT_c = \frac{E_{\text{Bind}}}{\ln(vb^2\rho l^2 D^{-2}\dot{\epsilon}^{-1})}, \quad (1)$$

where ρ is the density of moving dislocations; v , the Debye frequency ($\approx 10^{13} \text{ s}^{-1}$); b , the Burgers vector

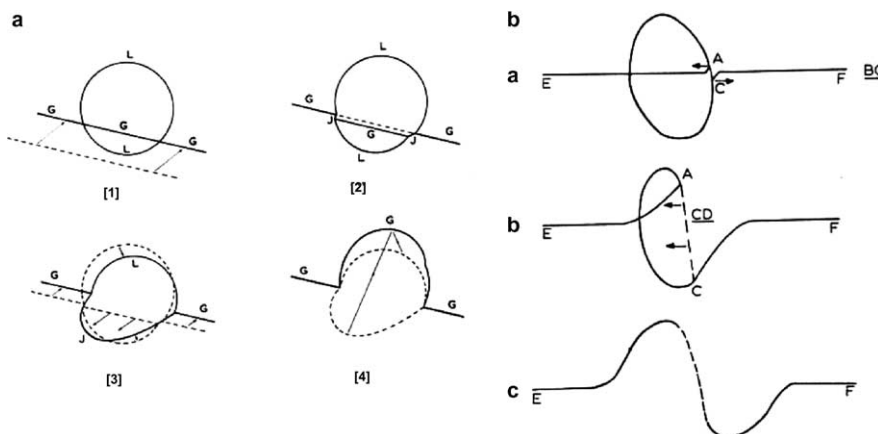


Fig. 2. Reaction-type interaction between a screw dislocation and a dislocation loop. (a) Foreman and Sharp mechanism [38]: when the loop (L) and the dislocation (G) are in contact, a junction dislocation (J) is formed. J and L rotate towards one another and combine to form a segment of the original dislocation G. (b) Hirsch mechanism [39]: a junction AC is formed at the point of contact. Nodes A and C are unstable and the dislocation segment AC sweeps across the plane of the loop which aggressively turns into the glide plane of A. When AC reached the opposite side a helix has been generated.

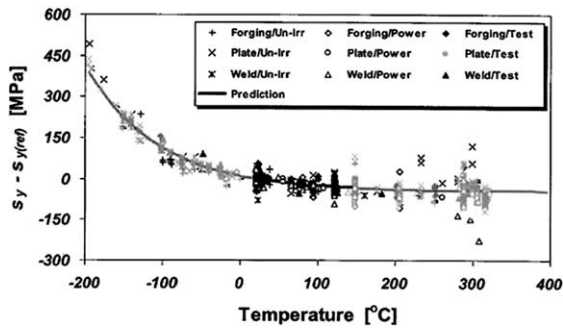


Fig. 3. Temperature-dependence of the yield stress of un-irradiated and irradiated iron-based alloys [42]. S_y : yield stress, $S_y(\text{ref})$: yield stress at about 27 °C.

(2.48×10^{-10} m for iron); $D = \left(\frac{2\pi l^4}{E_{\text{Bind}}}\right)^{\frac{1}{3}}$, the effective interdefect distance along the dislocation line resulting from the zig-zag shape of the dislocation; $l = (Nd)^{-0.5}$, the average interdefect distance; N , the number density of the defects; d , the diameter of the defects; T , the dislocation line tension, $T \approx \frac{\mu b^2}{2}$; μ , the shear modulus (8×10^{10} Pa); $\dot{\epsilon}$, the strain rate. With $\rho = 10^{14} \text{ m}^{-2}$, $N = 10^{25} \text{ m}^{-3}$, $d = 3 \times 10^{-9} \text{ m}$, $\dot{\epsilon} = 10^{-5} \text{ s}^{-1}$, this expression shows $E_{\text{Bind}} \approx -0.7 \text{ eV}$ at $T_c = 20 \text{ °C}$.

For RPV steels, the effect of the overcoming of irradiation-induced defects by thermal activation is difficult to assess experimentally. Indeed, as noticed by Kirk et al. [42], the temperature-dependence of the yield stress of such steels appears independent of the presence of the irradiation-induced damage (Fig. 3) for temperature higher than -200 °C . Kirk et al. suggested that the thermally activated overcoming of irradiation-induced defect is screened by the strong temperature-dependence imposed by the Peierls friction stress. Kirk et al.'s observation is coherent with Bacon and Osetsyky's simulation results [41] showing a low temperature-dependence of the resolved shear stress required to overcome small copper precipitates ($R \leq 1 \text{ nm}$) in iron at temperature higher than -173 °C .

2.3. Plasticity model in RPV-1

Simulation of irradiation-induced hardening is a complex task that can be done only by modeling the involved physical phenomena. This section describes the model used in RPV-1 to reproduce the plasticity behavior of irradiated RPV steels.

RPV-1 considers only four types of irradiation-induced defects [7]: spherical copper-rich precipitates containing Mn and Ni atoms, spherical vacancy clusters, spherical vacancy–solute atom (Cu, Mn, Ni) clusters and 2-D SIA-loops on $\{111\}$ habit planes with $\frac{1}{2}\langle 111 \rangle$ Burgers vector. It also relies on the following hypotheses [5,7]:

- the irradiation-induced increase of yield stress is independent of the pressure vessel steel type (forging, plate, weld) and weakly depends on the metallurgical structure. Only the grain (or lath) size and the dislocation density have an influence (effects of size and distribution of carbides, shape of grains, etc. are not accounted for);
- in its current version, RPV-1 does not take into account the intergranular embrittlement due to phosphorus segregation. Consequently, it cannot be used to forecast the behavior of steels containing more than about 150 ppm of phosphorus;
- the only chemical elements participating in the irradiation-induced damage are Cu, Mn and Ni. Si is not accounted for; carbon and nitrogen are indirectly taken into account by reducing the mobility of vacancies;
- in copper-rich precipitates and vacancy–solute atom (Cu, Mn, Ni) clusters, Ni and Mn atoms are supposed to have the same 'hardening effect' as copper atoms. Thus, for the hardening assessment, these defects are considered to contain only one type of solute atoms: copper atoms;
- the plasticity of irradiated RPV steels is controlled by the gliding of screw dislocations. This hypothesis is verified for non-irradiated RPV-steel at temperatures up to 20 °C but to our knowledge it has never been checked after irradiation;
- screw dislocations are considered to slip on the $\{110\}$ planes of bcc iron (e.g. [43–45]);
- the lattice friction (Peierls stress) exerted on the screw dislocation is supposed to be independent of the irradiation-induced defects.

In RPV-1 the assessment of the irradiation-induced hardening is achieved with a Foreman and Makin-type code [46], called DUPAIR [5,47]. Such a code is aimed at assessing the increase of the resolved shear stress of a single grain, due to obstacles which oppose to the gliding of one dislocation. The increase of the macroscopic yield stress is calculated by multiplying the obtained result by the Schmid's factor (≈ 3).

DUPAIR relies on several hypothesis and simplifications which are well described in the literature (e.g. [46]). The most important ones are the following:

- the grain is described by its shear modulus and Poisson's ratio;
- the dislocation is described by its line tension and Burgers vector;
- the line tension is independent of the curvature of the dislocation. Consequently, when an external stress is applied, each dislocation segment between two obstacles bows with a circular curvature. This is a strong approximation, particularly when the Peierls friction stress is high: e.g. screw dislocation in Fe below room temperature;

- three models of line tension can be used in DUPAIR:
 - Model 1 supposes that the line tension is independent of the character (edge, screw or mix) of the dislocation segments and is given by $T = \frac{\mu b^2}{2}$ (e.g. [48]). It is the model that Foreman and Makin used to develop their code [46,49].
 - Model 2 is more realistic since it takes into account the character of the dislocation segments in their straight configuration (before applying the stress). It considers that the line tension along these segments is given by the Wit and Koehler's expression [5,6,8,9]: $T(\theta) = \frac{\mu b^2}{4\pi} \left(\frac{1+\nu-3\nu\sin^2\theta}{1-\nu} \right) \ln \left(\frac{A}{r_0} \right)$, where r_0 is the core radius; θ , the angle between the segment line in its straight configuration and the Burgers vector; ν , the Poisson's ratio (≈ 0.3) and A , an outer cutoff distance $= L - 2r$, L is the distance between the center of the two obstacles pinning the segment and r is the average radius of these obstacles in the slip plane.
 - Model 3 also relies on the Wit and Koehler expression, but in this case the value of A is calculated from the expression proposed by Bacon et al. [50]: $A = \frac{1}{(2r)^{-1} + (L-2r)^{-1}}$.
- the obstacles are supposed to be pinning points and are characterized by the pinning force they exert on the dislocation line;
- only one dislocation moves and cannot leave its slip plane (no cross-slip or climbing);
- the dislocation can overcome any obstacle as soon as one of the following conditions is fulfilled:
 - the resultant of the line tension of the two segments on each side of the obstacle is higher than the pinning force.
 - the two segments on each side of the obstacle are parallel (Orowan process).

The input parameters of DUPAIR are the number density of each type of obstacles, the radius of each obstacle and the force exerted by each obstacle on the dislocation.

3. Simulations and experimental work carried out

This section presents the work carried out (i) to assess the pinning forces exerted by the irradiation-induced defects on a screw dislocation and (ii) to validate the approach used in RPV-1 to reproduce the irradiation-induced hardening (use of DUPAIR with the assessed pinning forces).

3.1. Method to characterize the pinning forces

To build RPV-1, the interactions between irradiation-induced defects and a screw dislocation were assessed from molecular dynamics simulations at 0 K

using a 'static approach'. That means that the dislocation remains fixed in the simulated crystal (only displacements of atoms related to the crystal relaxation are allowed) and different positions of the defects as regard to the dislocation are considered. This approach can be summarized in the following way [3,15,51]:

- the screw dislocation is introduced at the center of the simulated crystal and its displacement field is applied to the atoms;
- the studied defect is successively introduced at different distances from the dislocation line (one simulation per position of the obstacle);
- for each configuration, a quasi-Newton quenching is used to obtain equilibrium atomic arrangement: atomic velocities are rescaled every time step ($\approx 10^{-15}$ s) to reach a steady energy of the system (at ± 0.01 eV) at the simulation temperature ($T = 0$ K). Typically, the static equilibrium arrangement is obtained after about 1000 simulation steps;
- the relaxed energy of the system is then recorded versus the distance between the core of the obstacle and the dislocation line. For a given configuration, the interaction energy between the two features is defined as the relaxed energy for the considered configuration minus the relaxed energy when they are largely separated (i.e. do not interact).

Four types of defects were considered: SIA loops, copper precipitates, copper–iron clusters and vacancy clusters.

The simulations were carried out in pure α Fe or α binary Fe–Cu alloys with the molecular dynamics code DYMOKA developed by EDF [52]. The EAM-type Fe, Cu and Fe–Cu atomic potentials used for the simulations were developed by Ludwig et al. [53] and hardened by EDF for simulation of displacement cascades. They lead to the following characteristics at 0 K:

- lattice parameter: $a_0 = 0.287$ nm for bcc Fe; $a_0 = 0.288$ nm for bcc Cu;
- interface energy between bcc copper and bcc iron: 318 and 121 mJ m⁻² on the {100} and {110} planes, respectively;
- interface energy of a spherical bcc copper precipitate of 2 nm radius: 207 mJ m⁻².

The simulated crystal has its edges along the [112], $[\bar{1}10]$ and [111] directions, and respectively 26, 22 and 26 elementary cells in the three directions. Usual boundary conditions for static studies of dislocation were applied: i.e. periodic along the dislocation line (direction [111]) and layers of fixed atoms along the surfaces perpendicular to the two other directions (width of these

layers: $a_0\sqrt{2}$ and $a_0\sqrt{6}$ for surfaces perpendicular to $[1\bar{1}2]$ and $[\bar{1}10]$, respectively).

Dislocation: only a right-handed screw dislocation with Burgers vector $b = 1/2 [111]$ was considered in the simulations. As observed by Suzuki et al. [54], two distinct types of site are possible to place the elastic center of a screw dislocation. The introduction of a right-handed screw dislocation in both types of site leads to different atomic configurations termed ‘easy’ and ‘hard’ respectively [55]. Suzuki et al. as well as Harry and Bacon noticed [54,15] that the easy configuration is energetically more favorable and that a dislocation which is initially in a hard configuration may shift to the easy one. In the present study, the dislocation was always placed in an easy configuration. The site was selected in such a way that the dislocation line was close to the central axis of the simulated crystal.

The dislocation was introduced by applying to the atoms the isotropic elastic displacement field of a screw dislocation in α iron [33]. Following established practice, the core structure of the dislocation was analyzed by plotting the $[111]$ displacement difference between pairs of atoms with arrows drawn between them (to get the so-called differential displacement maps). As it is well known (e.g. [56,15]), the atomic registry in the dislocation core appeared concentrated along the $\{110\}$ planes of the $[111]$ zone. The center of the dislocation can be regarded as the intersection of three stacking faults with displacement $1/6 [111]$. On each of the three $\{110\}$ planes, the large relative displacements occur only on one side of the dislocation, resulting in a three-fold symmetry.

In an isotropic crystal, the elastic energy per unit length of a screw dislocation is given by: $E = \frac{ub^2}{4\pi} \ln\left(\frac{A}{r_c}\right) + E_c$, where r_c and A are the core radius and the outer cutoff distance, respectively (e.g. [57,58]). To determine r_c , molecular dynamics simulations were carried out [59] so as to calculate the energy in different cylinders of radius A around the dislocation. The plot of the results leads to estimate $r_c \approx 8 \text{ \AA}$, which is larger than the radius of some neutron-irradiation induced defects considered in the following.

SIA loops: the dislocation loops were introduced in the simulated crystal by: (i) making a selection of atoms on three successive $\{111\}$ planes, these atoms were on filled hexagonal shells surrounding a central atom, and (ii) by moving a copy of the selected atoms a distance $+b/2$ along the normal of the planes, and moving back the selected atoms a distance $-b/2$. After the introduction of the loop, the crystal was quenched. In their minimum energy configuration, the loops are made of $\langle 111 \rangle$ crowdions disposed on several (up to 7) parallel $\{111\}$ planes. They are more extended than perfect planar loops which should be located on only three planes. On a $\langle 111 \rangle$ projection, loops have an hexagonal shape, with edge parallel to $\langle 112 \rangle$ directions.

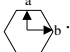
Among the possible $\{111\}$ habit planes, only two were considered here: (111) , leading to a loop and a dislocation with parallel Burgers vectors, and $(1\bar{1}\bar{1})$ leading to an angle of about 70° between the Burgers vectors. For each plane, five loops were taken into account (Table 1). They were placed in the simulated crystal so that their center was on the slip plane of the dislocation. The relative positions were noted as shown in Fig. 4 and about 20 values (0, positive and negative) of x were used for each loop.

Copper-rich precipitates and vacancy-clusters: as aforementioned, we consider that in copper-rich precipitates, Mn and Ni atoms have the same hardening effect as copper atoms. Consequently, only pure copper precipitates were taken into account to assess the pinning forces exerted by precipitates. Their radii, given in Table 2, are lower than the critical radius of 3 nm for which the structural transformation bcc structure \rightarrow 9R structure occurs [12,60]. The considered precipitates were thus expected to have a bcc structure, some of them being smaller than the dislocation core radius. The relative positions of the precipitates, the dislocation line and the slip plane were noted as shown in Fig. 5. For each defect, simulations were carried out with six positive values of y along $[1\bar{1}0]$; for each of these values, 20 values of x (0, positive and negative values) were used along $[112]$.

Simulations were also carried out with clusters (radius = 1.12 nm, 500 atoms) composed of an homogeneous mixture of Cu and Fe atoms. Ten copper contents were considered: 5%, 10%, 15%, 20%, 25%, 30%, 35%, 50%, 75% and 100%. Only the configuration where the slip plane is through the center ($y = 0$) of the cluster was allowed for (Fig. 5).

Table 1
SIA loops considered

Number of SIA's in the loop	7	19	37	61	91
a (nm)/ b (nm) ^a	0.2/0.35	0.4/0.7	0.6/0.0	0.8/0.4	1.0/3.5

^a a and b are defined as followed: 

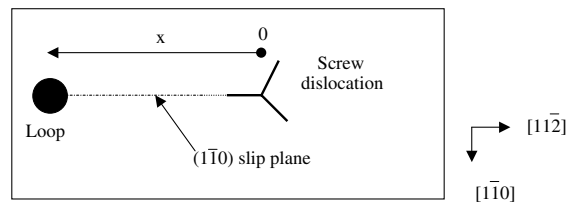


Fig. 4. Relative position of the dislocation loop [here on (111) habit plane] and the screw dislocation. The slip plane of the dislocation is through the center of the loop.

Table 2
Copper precipitates and vacancy clusters considered in the simulations

Number of copper atoms or vacancies in the defect	10	50	100	200	500	750	1000	2000	3000	4000
Radius of the defect (nm)	0.30	0.52	0.65	0.82	1.12	1.28	1.41	1.77	2.03	2.23
Copper precipitates taken into account	–	X	X	X	X	–	X	X	X	X
Vacancy clusters taken into account	X	X	X	X	X	X	X	X	–	X

X: taken into account.

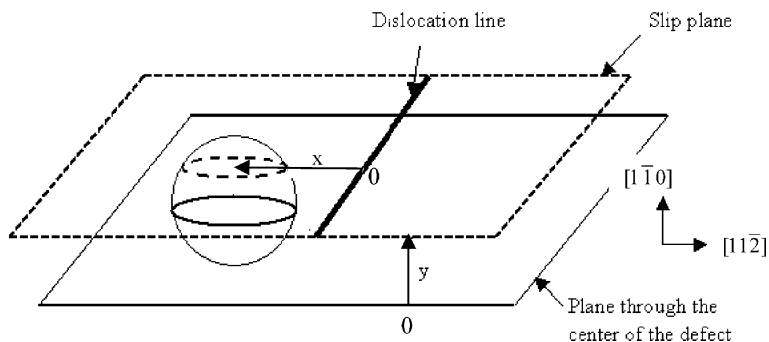


Fig. 5. Relative positions of the dislocation line, slip plane and copper precipitate, vacancy clusters or copper–iron clusters.

Nine spherical vacancy clusters were also considered, their size is given in Table 2. Some of them are also smaller than the dislocation core. The corresponding simulations were similar to those described for the copper precipitates.

3.2. Experimental validation

We attempted to validate the approach used in RPV-1 to simulate grain hardening (use of DUPAIR with the assessed pinning forces) by comparing simulation results with previously published experimental results. The challenge was to find out available results of tensile tests carried out on iron-based alloys for which a complete description of the hardening defects was available. The possibilities were very limited and we had to separate the validation for copper precipitates on the one hand from vacancy clusters and SIA loops on the other hand.

For the copper precipitates: results obtained by Goodman et al. and by Mathon on Fe–1.5%Cu alloys thermally aged at 500 °C were used. It is well known that at this temperature such alloys exhibit a hardening resulting from the precipitation of copper precipitates. Goodman et al. [61] characterized this hardening by tensile tests at 20 °C and Mathon [62] by hardness tests. Both teams characterized the copper precipitates by small angle neutron scattering (SANS).

To supplement these previous studies, we established a relationship between hardness and yield stress for this type of alloy and got precise information on the chemical composition of the precipitates by carrying out tensile tests, hardness tests and atom probe experiments

on a Fe–1.5%Cu alloy aged 1.5, 2.5 and 25 h at 500 °C. The mechanical tests were performed in the Laboratoire de Métallurgie Physique et Génie des Matériaux of the University of Lille and the Atom Probe examinations in the Groupe de Physique des Matériaux of the University of Rouen [63].

For the vacancy clusters and SIA loops: the results of tensile tests, TEM experiments and positron annihilation experiments obtained by Eldrup et al. on a pure iron neutron-irradiated in HIFR at 70 °C [64] probably constitute the most complete set of experimental data which can be used. Unfortunately, the microstructural data do not include any information on SIA-loops with a radius smaller than 1 nm. Such loops make a significant contribution to irradiation-induced hardening and cannot be neglected for the simulation of this hardening. Anyhow, the Eldrup et al. results were used, keeping in mind that the irradiation-increases of yield stress simulated from their data should underestimate the measured ones.

4. Results

4.1. Interaction between the dislocation and SIA loops

When the dislocation is outside the SIA loop, the interaction energy between the two defects is almost negligible, except when they are almost in contact. In this configuration, they attract each other and have a ‘reaction’-type interaction. Two cases have to be considered.

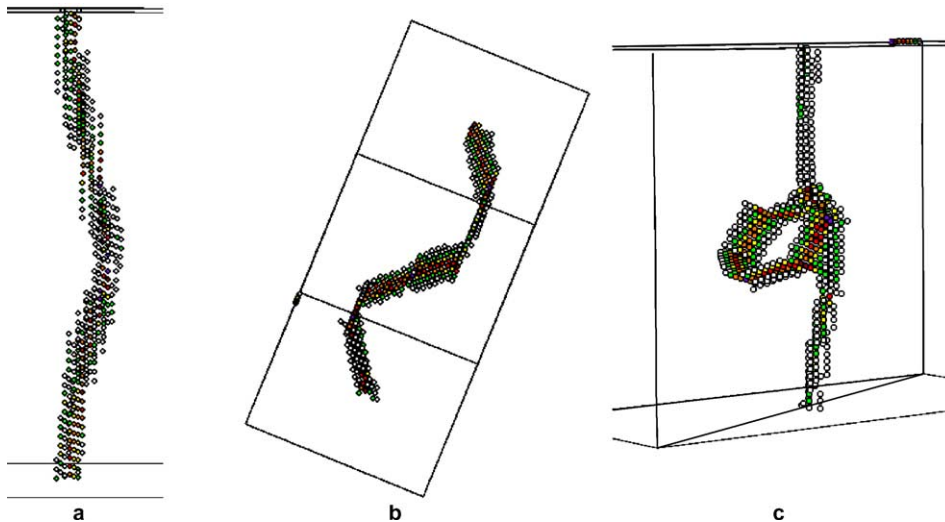


Fig. 6. Formation of an helix or a junction by a screw dislocation and a SIA loop. (a) helix (19 SIA loops), (b) helix (217 SIA loops) and (c) junction (217 SIA loops).

Screw dislocation and SIA loops with parallel Burgers vectors: when both defects have parallel Burgers vector, their combination leads to the transformation of the loop into an helix on the dislocation (Fig. 6(a) and (b)), as foreseen by Hirsch (see Fig. 2(b)). An example of ‘interaction energy versus distance’ curve is given in Fig. 7. It can be seen that in accordance with the isotropic elasticity calculations (see Section 2.1), the interaction between both defects is negligible when they are not in contact.

Screw dislocation and SIA loops with non-parallel Burgers vectors: when the Burgers vectors are non-parallel

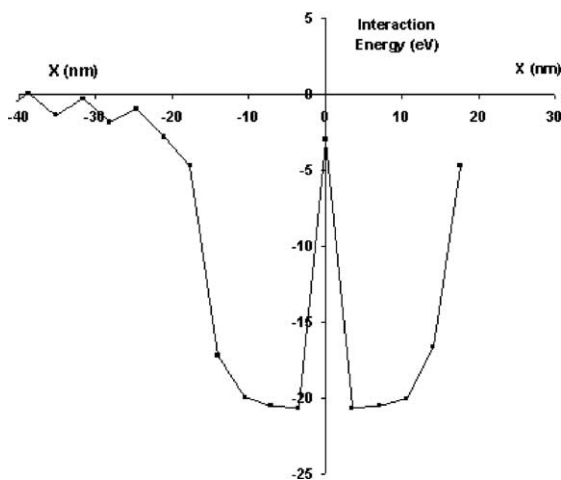


Fig. 7. Interaction between a screw dislocation and loops containing 37 SIAs.

(angle $70^{\circ}32'$), the dislocation and the loop interact in two ways according to the size of the loop (Fig. 6(c)):

- small loops (≤ 19 SIAs) rotate to have their Burgers vector parallel with that of the dislocation. Then, they combine with the dislocation, which leads to their destruction and the formation of an helix on the dislocation;
- large loops (> 19 SIAs) form a junction with the dislocation, along $[111]/\sqrt{3} + [\bar{1}10]/\sqrt{2}$ directions.

4.2. Interactions with copper precipitates, copper–iron clusters and vacancy clusters

Fig. 8 sketches (for a given value of y) typical curves giving the evolution of the interaction energy (E_{Inter}) versus the distance between the dislocation and a copper precipitate, a vacancy cluster or a copper–iron cluster. In spite of the non-symmetry of the interaction configuration (for $x > 0$, the defect is facing one fractional dislocation; for $x < 0$, it is facing two fractional dislocations, see Fig. 4), most of the obtained profiles are almost symmetrical. In all cases, E_{Inter} is minimal (hence the interaction is maximal) when the dislocation is within the obstacle, which means that the latter attracts and pins the dislocation. The zone corresponding to the minimal energy increases with the size of the obstacle. The binding energy (E_{Bind}) between the two features is defined as the minimal interaction energy.

To determine the pinning forces exerted by the obstacles on the dislocation, Gaussian curves having the following expression were fitted on the simulation results:

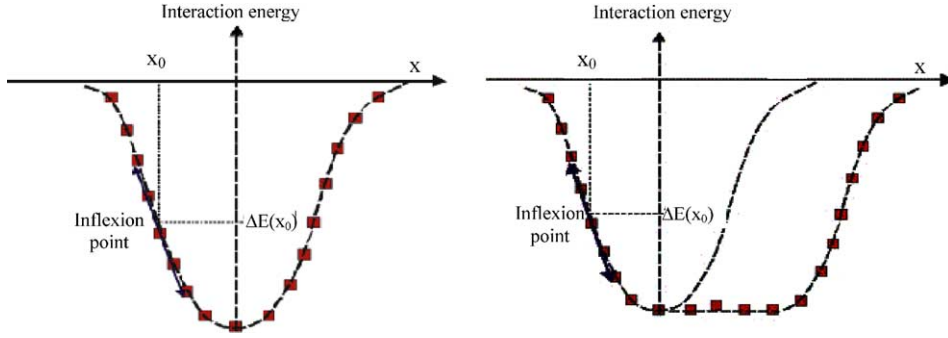


Fig. 8. Schematic draw showing the evolution of the interaction energy versus the distance between the dislocation and a large or small copper precipitate, vacancy cluster or copper–iron cluster. A Gaussian curve was fitted on the simulation results: all the results for smallest precipitates and only results corresponding to one side of the plateau of minimal interaction energy for the largest ones.

$$E_{\text{Inter}}(r, x, y) = E_{\text{Bind}}(y, r) \exp[-\alpha(r, y)x_2], \quad (2)$$

where x and y are defined in Fig. 5, r is the radius of the obstacle, α is a parameter depending on r and y . As shown in Fig. 8 all the results were used for the small defects and only results corresponding to one side of the plateau of minimal energy were taken into account for the largest ones. The pinning force was defined as the value of the derivative of the Gaussian at the inflexion point ($x_0 = \sqrt{\frac{1}{2\alpha(r, y)}}$):

$$F = -2\alpha(r, y)x_0 E_{\text{Bind}}(y, r) \exp[-\alpha(r, y)x_0^2]. \quad (3)$$

For copper precipitates: all the studied pure copper precipitates have a bcc structure when they are not in contact with the dislocation. As observed by Harry and Bacon [15], when the dislocation line is within a precipitate, its core spreads and modifies the precipitate's bcc structure. Examples of curves 'interaction energy versus distance' are given in Fig. 9 for two copper precipitates. In all cases, the minimal binding energy (hence the maximal interaction) and the maximal pinning force ($F_{\text{Pm}}^{\text{Cu}}$) are obtained when the slip plane is through the center of the precipitate ($y = 0$); the values are given in Table 3. Analysis of the results shows that:

- the maximal pinning force and the precipitate radius are linked by the expression:

$$F_{\text{Pm}}^{\text{Cu}} \approx 0.05r^{1.17} \quad (\text{eV}/\text{\AA}) \quad (r \text{ in } \text{\AA}) \quad (4)$$

- the pinning force evolves with y according to the expression:

$$F_{\text{P}}^{\text{Cu}} \approx F_{\text{Pm}}^{\text{Cu}} \exp(-0.843r^{-4.53}y^4) \quad (\text{eV}/\text{\AA}) \quad (r \text{ in } \text{\AA}) \quad (5)$$

Expression (5) is plotted in Fig. 10(a) for several size of precipitate. Irradiation-induced copper-rich precipitates ($r \leq 1.5$ nm) can be considered as rather weak obstacles.

For copper–iron clusters: examples of 'interaction energy versus distance' curves are given in Fig. 11. The binding energies and the pinning forces are given in

Table 4. Analysis of the results showed that the pinning force evolve linearly with the copper content in the cluster according to the following expression:

$$F_{\text{Pm}}^{\text{Cu-Fe}} \approx 0.013[\% \text{Cu}] \quad (\text{eV}/\text{\AA}). \quad (6)$$

This expression has been obtained for $y = 0$, but it can be supposed that a linear relation between the pinning force and the copper content can also be applied for $y \neq 0$.

For vacancy clusters: examples of 'interaction energy versus distance' curves are given in Fig. 12 for two vacancy clusters. In all cases, the minimal binding energy (hence the maximal interaction) and maximal pinning force are obtained when the slip plane is through the center of the cluster ($y = 0$); the values are given in Table 5. Analysis of the results shows that:

- the maximal pinning force $F_{\text{Pm}}^{\text{Va}}$ and the cluster radius are linked by the expression:

$$F_{\text{Pm}}^{\text{Va}} \approx 0.0448r^{1.23} \quad (\text{eV}/\text{\AA}) \quad (r \text{ in } \text{\AA}) \quad (7)$$

- the pinning force evolves with y according to the expression:

$$F_{\text{P}}^{\text{Va}} \approx F_{\text{Pm}}^{\text{Va}} \exp(-0.219r^{-1.74}y^2) \quad (\text{eV}/\text{\AA}) \quad (r \text{ in } \text{\AA}) \quad (8)$$

The expression (8) is plotted in Fig. 10(b) for several sizes of cluster. It can be noticed that results are quite similar with those obtained for copper precipitates. For the clusters containing less than about 100 vacancies, the pinning forces are in agreement with that proposed by Bullough and Newman (see Section 2.1). Irradiation-induced vacancy clusters ($r \leq 0.5$ nm) can also be considered as rather weak obstacles.

5. Pinning forces used in RPV-1

The pinning forces used in RPV-1 to simulate the irradiation-induced hardening of RPV steels at 20 °C

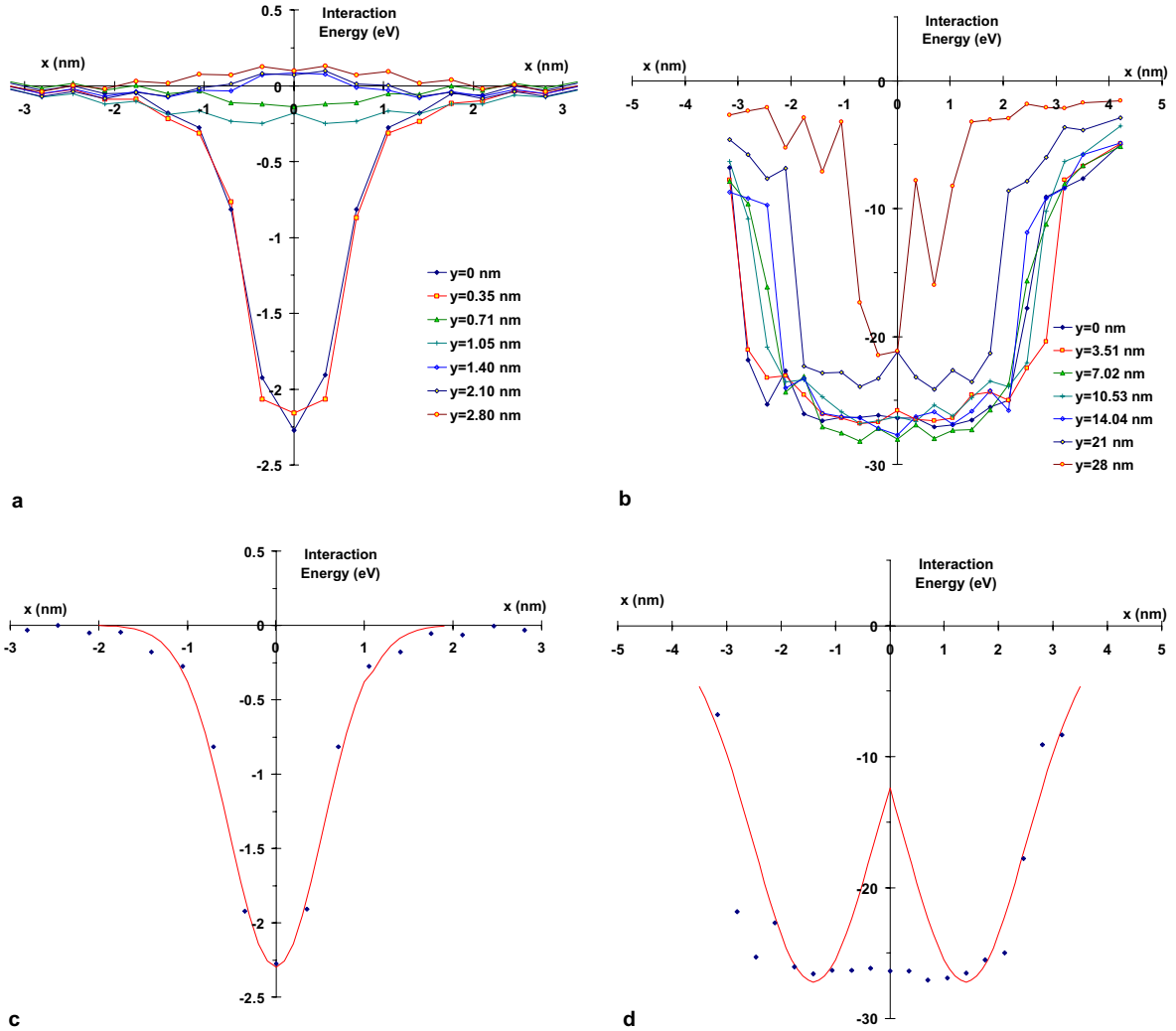


Fig. 9. Examples of results obtained for the copper precipitates (x and y are defined in Fig. 5): (a, c) curves “interaction energy versus distance” and (c, d) Gaussian curves fitted on simulation results obtained with $y = 0$.

Table 3

Minimal binding energy and maximal pinning force exerted by copper precipitates on a screw dislocation ($y = 0$)

Number of copper atoms in the precipitate	50	100	200	500	750	1000	2000	3000
Radius of the precipitate (nm)	0.52	0.65	0.82	1.12	1.28	1.41	1.72	2.03
Minimal binding energy (eV)	-2.27	-4.2	-4.8	-10	-11.6	-14.5	-21	-27
Maximal pinning force: $F_{\text{Pm}}^{\text{Cu}}$ (eV/Å)	0.35	0.45	0.60	0.85	1	1.12	1.46	1.71

are summarized in Table 6. Their estimation from molecular dynamics simulations at 0 K, as presented in Section 4, required some new approximations which are given in this paragraph. In a first step, we derive the pinning forces at 0 K, then we take into account the thermal activation and approximate them at 20 °C.

5.1. Pinning forces at 0 K

SIA loops: by interacting with a SIA-loop, a screw dislocation forms either a junction or an helix. We consider that the pinning force of the junctions is $F_{\text{P}}^{\text{Loop}} \approx \mu b^2/8$ (see Section 2.1). At 0 K, the helices are probably much stronger obstacles, leading to an Orowan mechanism [65].

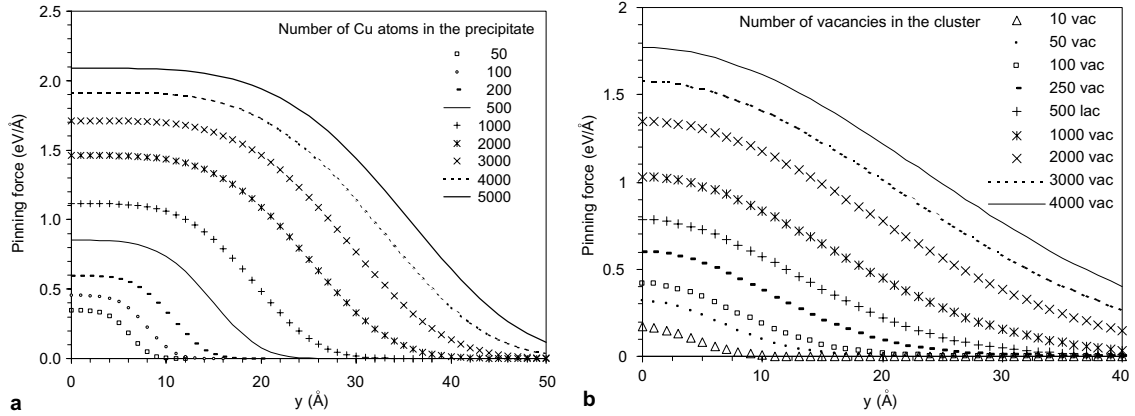


Fig. 10. Evolution of the pinning force versus the position of the slip plane (y) for different size of copper precipitates (a) or vacancy clusters (b) (y is defined in Fig. 5).

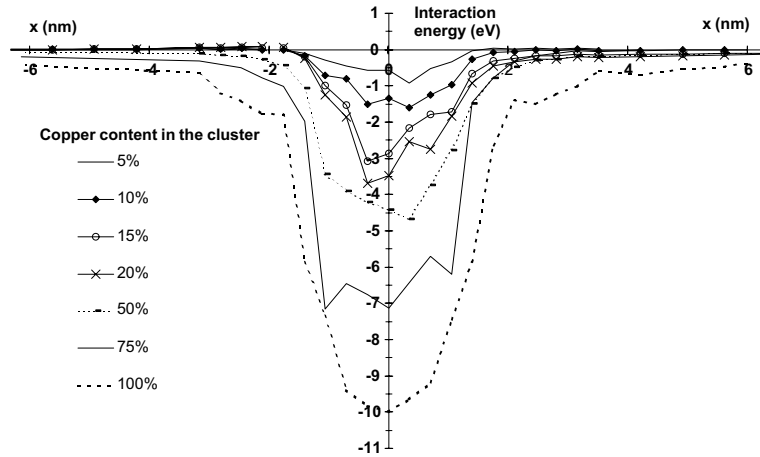


Fig. 11. Examples of curves 'interaction energy versus distance' for a screw dislocation and iron-copper clusters containing 500 atomic sites ($r = 1.18$ nm).

Table 4

Binding energy and pinning force ($y = 0$) exerted by iron-copper clusters ($r = 1.12$ nm, 500 atomic sites) on a screw dislocation

Percentage of copper in the cluster (%)	5	10	15	20	25	30	35	50	75	100
Minimal binding energy (eV)	-0.9	-1.6	-3.1	-3.6	-3.9	-4.3	-4.9	-4.7	-7.2	-9.9
Maximal pinning force: F_{Pm}^{Cu-Fe} (eV/Å)	0.08	0.15	0.18	0.32	0.33	0.49	0.57	0.515	0.831	1.09

Copper-rich precipitates: as aforementioned, we consider that in the copper-rich precipitates Mn and Ni atoms have the same 'hardening effect' as copper atoms. Thus, the pinning forces exerted by such precipitates at 0 K are calculated by replacing their Mn and Ni atoms by Cu atoms and using expression (5).

Vacancy-clusters: the pinning forces (F_p^{Va}) exerted at 0 K by the vacancy clusters can be calculated with expression (8).

Vacancy-solute atom clusters: having no model to assess the pinning forces (F_p^{Va-sol}) exerted by the vacancy-solute atom clusters, these forces are assessed by replacing Mn and Ni atoms by Cu atoms and by using the expression:

$$F_p^{Va-sol} \approx (F_p^{Cu} + F_p^{Va})/2, \quad (9)$$

where F_p^{Cu} and F_p^{Va} are given by (5) and (8).

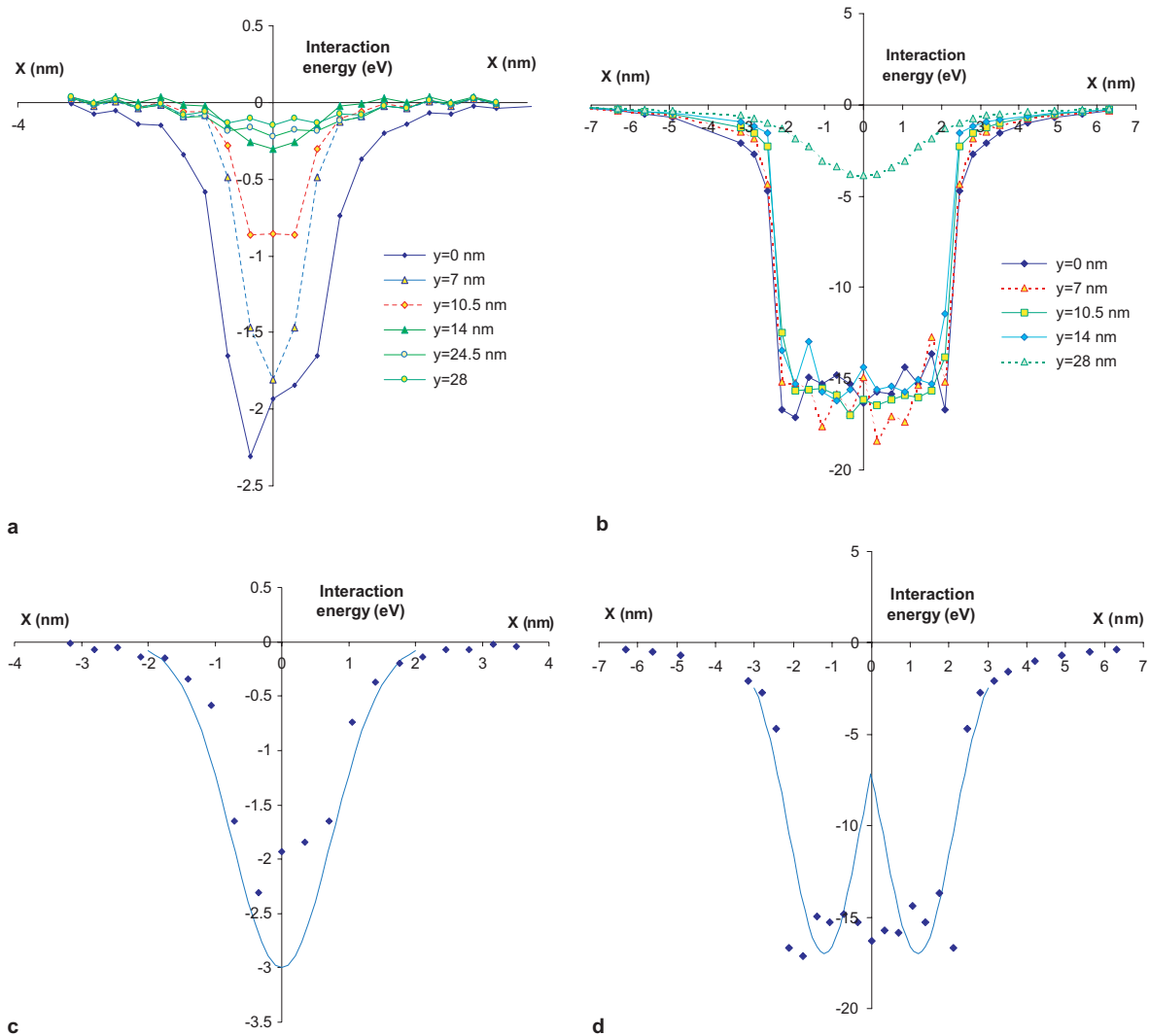


Fig. 12. Examples of results obtained for the vacancy clusters (x and y are defined in Fig. 5): (a, b) curves 'interaction energy versus distance' and (c, d) Gaussian curves fitted on simulation results obtained with $y = 0$.

Table 5

Minimal binding energy and maximal pinning force exerted by vacancy clusters on a screw dislocation ($y = 0$)

Number of vacancies in the cluster	10	50	100	200	500	1000	2000	4000
Radius of the cluster (nm)	0.30	0.52	0.65	0.82	1.12	1.41	1.78	2.03
Minimal binding energy (eV)	-1.2	-2.3	-4	-6	-8.5	-12.4	-16	-24
Maximal pinning force: F_{Pm}^{Va} (eV/Å)	0.17	0.32	0.429	0.55	0.78	1.03	1.35	1.77

5.2. Thermal activation

SIA loops: we consider that at 20 °C thermal fluctuations do not help significantly the screw dislocations to escape from the junctions they formed with SIA loops. However, we suppose that the helices disappear shortly

after their creation and then do not exert any significant pinning force. Indeed, an helix on a screw dislocation may be described as a succession of kinks on $\{110\}$ slip planes (see sketch in Fig. 13). As recently confirmed by molecular dynamics simulations [45], kinks are very mobile along screw dislocation lines in iron at room

Table 6
Summary of the pinning forces used to simulate the irradiation-induced hardening at 20 °C with RPV-1

Defect	Size of the defect ^a	Force (eV/nm) with r in Å
SIA loops	$N < 19$	$F_P^{\text{Loop}} = 0$
	$N \geq 19$	$F_P^{\text{Loop}} = 0$ for parallel Burgers vectors (formation of an helix); applies to one-quarter of the loops $F_P^{\text{Loop}} = \mu b^2/8$ for non-parallel Burger vectors (formation of a junction); applies to three quarters of the loops
Copper-rich precipitates	$N < 6$	Copper atoms contribute the solution hardening
	$N \geq 6$	$F_P^{\text{Cu}} = 1.3 F_{\text{pm}}^{\text{Cu}} \exp(-0.843 r^{-4.53} y^4)$ with $F_{\text{pm}}^{\text{Cu}} = 0.39 r^{1.17}$
Vacancy clusters	$N < 6$	$F_P^{\text{Va}} = 0$
	$N \geq 6$	$F_P^{\text{Va}} = 1.2 F_{\text{pm}}^{\text{Va}} \exp(-0.219 r^{-1.74} y^2)$ with $F_{\text{pm}}^{\text{Va}} = 0.373 r^{1.23}$
Vacancy–solute atom clusters	$N < 6$	$F_P^{\text{Va-sol}} = 0$
	$N \geq 6$	$F_P^{\text{Va-sol}} = (F_P^{\text{Cu}} + F_P^{\text{Va}})/2$

^a N = number of cu atoms or vacancies in the defect.

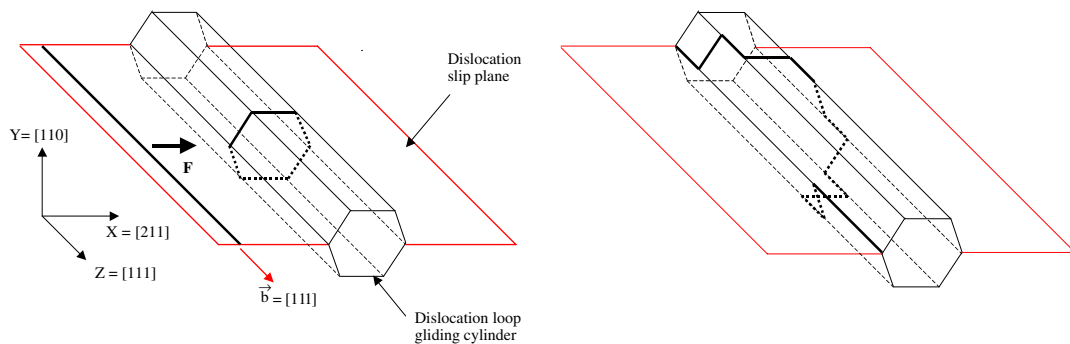


Fig. 13. Sketch showing a screw dislocation interacting with SIA loops (habit plan perpendicular to the dislocation line) and forming an helix described as a succession of kinks on $\{110\}$ slip planes. Both defect have parallel Burgers vectors.

temperature. At this temperature, screw dislocation lines are mostly straight in irradiated RPV steels (the Peierls friction stress is still efficient and the dislocations are slightly bowed between the irradiation-induced defects since they are weak obstacles), then the applied shear stress can easily sweep the kinks along them. Whatever the applied stress, two configurations have to be taken into account according to the relative orientation of the applied stress and the dislocation line orientation (cf. Peach and Kohler force):

- all the kinks forming the helix are swept to the extremities of the dislocation segments where they may be absorbed by sinks (grain boundaries, carbide–matrix interfaces, etc.), which makes the helix vanish (Fig. 14). At the end of the process, the loop has disappeared and the dislocation line has regained its straight configuration;
- two kinks forming the helix slip in opposite directions and create a cross-kink (Fig. 15). As proposed by Marian et al. [45], kinks slipping from other parts

of the dislocation line may suppress the cross-kink and rebuild the loop behind the dislocation. These slipping kinks may be generated in other parts of the dislocation (e.g. by thermal activation or by other helices).

In conclusion, we consider that at 20 °C:

- the loops containing more than 19 SIAs and with a Burgers vector non-parallel to that of the dislocation (see Section 4.1) lead to the formation of junctions and exert a force $F_P^{\text{Loop}} \approx \mu b^2/8$;
- the loops with less than 19 SIAs as well as the larger loops with a Burgers vector parallel to that of the dislocation (see Section 4.1) lead to the formation of helices and do not exert any pinning force on the dislocation ($F_P^{\text{Loop}} \approx 0$).

Copper-rich precipitates, vacancy clusters and vacancy–solute atom clusters: as explained in Section 2.2, thermal activation can reduce the critical shear stress

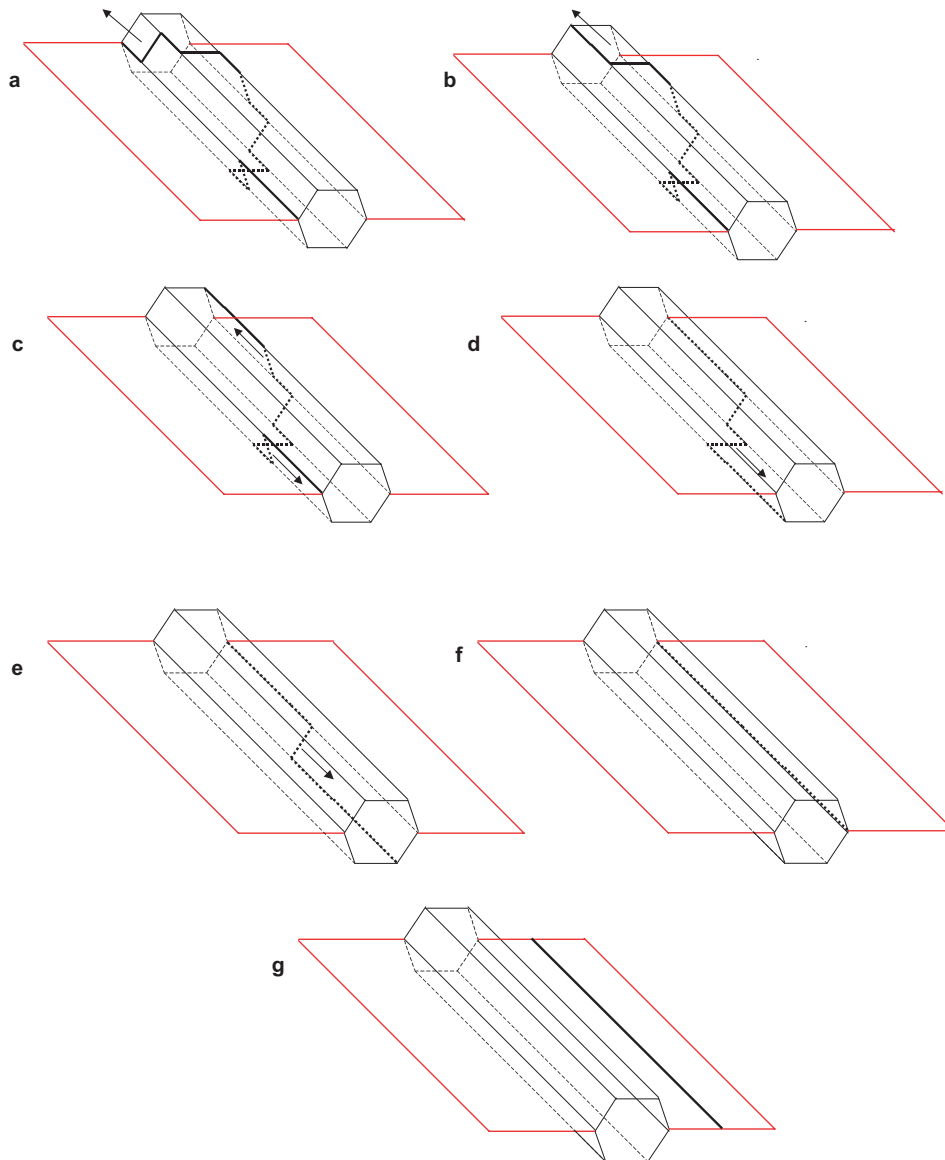


Fig. 14. Disappearance of a loop on a screw dislocation by gliding of kinks away from the loop area (the arrows indicates the directions of gliding of the kinks), vectors are given in Fig. 13.

of irradiated RPV-steels either by modifying the interaction mechanism between the defects and the dislocations or by inducing atomic fluctuations large enough to help the dislocations to overcome the smallest defects. To assess the pinning forces exerted at 20 °C by the copper-rich precipitates, vacancy clusters and vacancy–solute atom clusters, we consider only this last mechanism. In particular, for the copper-rich clusters and vacancy–atom clusters, we do not introduce the temperature dependence observed by Bacon and Ossetsky in the case of pure copper precipitates (see Section 2.2), for at least two reasons:

- the considered irradiation-induced defects are small (core zone of about 1 nm for the copper-rich precipitate) or contain a high concentration of iron atoms (about 80% for the vacancy–solute atom clusters), thus their tendency for bcc-to-fcc transformation must be weak whatever the temperature;
- since we consider a screw dislocation, we do not expect any significant climbing effect during the overcoming of the defects.

It will be seen in Section 5.3, that neglecting the pinning force temperature dependence measured by Bacon and

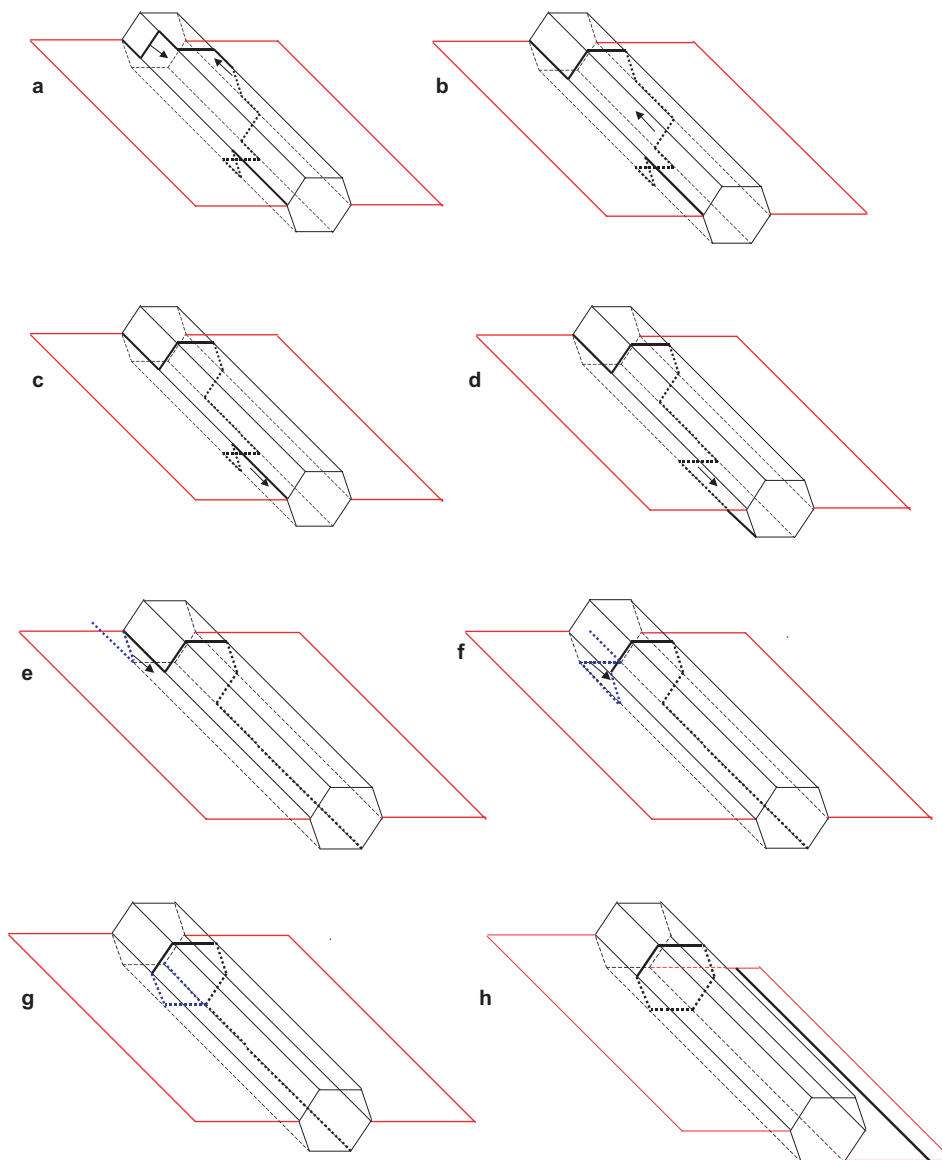


Fig. 15. Reconstruction of a loop from an helix on a screw dislocation by gliding of kinks away and to the loop area (the arrows indicate the directions of gliding of the kinks, the blue kinks are coming from other parts of the dislocation line), vectors are indicated in Fig. 13. (For interpretation of colors in this figure legend, the reader is referred to the web version of this article.)

Osetsky for an edge dislocation, does not affect the quality of our simulations even for large ($r \approx 1$ nm) pure copper precipitates. This observation may indicate that this temperature dependence is weaker for screw dislocations than for edge ones.

In Section 2.2, it was estimated that at 20 °C the dislocations can overcome defects with a binding energy higher than about -0.7 eV without the help of the stress. This binding energy corresponds to vacancy-clusters, copper-rich precipitates and vacancy-solute atom clusters containing less than about five solute

atoms or vacancies. Consequently, we consider that such defects do not introduce any hardening at 20 °C. The solute atoms they contain are supposed to be in solution and to contribute to the athermal solution hardening.

5.3. Validation

As demonstrated hereafter, the comparison with experimental results shows that the simplified approach used in RPV-1 to simulate grain hardening (use of

Table 7
Increase of hardness and yield stress of a Fe–1.5%Cu alloy during ageing

Ageing time (h)	ΔH_v	$\Delta R_{p0.2}$ (MPa)
1.5	117	292
2.5	108	270
25	103	257

DUPAIR with the assessed pinning forces) leads to reasonable results.

Copper precipitates: the tensile and hardness tests carried out on the Fe–1.5%Cu alloy aged 1.5, 2.5 and 25 h at 500 °C (Table 7) show that increases of hardness and yield stress resulting from the copper precipitation in this alloy verify the following relation:

$$\Delta R_{p0.2} = 2.5\Delta H_v. \quad (10)$$

The tomographic atom probe experiments on the same alloy reveal that the copper content in the precipitates is about 85% after the 1.5 h ageing time and 100% for the 2.5 and 25 h ageing times.

Results previously obtained by Goodman et al. [61] and Mathon [62] on aged Fe–1.5%Cu alloys are summarized in Table 8. In all cases, the precipitates have an average radius much lower than the critical value of 9 nm from which a transformation of their bcc structure into a 9R structure is expected. Therefore, the pinning forces derived in this study can be used to describe their interaction with a screw dislocation. Expression (10) was used to determine the increase of yield stress of the alloy studied by Mathon from the hardness data. The obtained values are plotted in Fig. 16 with those published by Goodman et al. and those measured in this study. All the results are consistent.

For each ageing time, the number density and average radius of the precipitates determined by Goodman et al. and Mathon (SANS experiments) were used as input parameters of the DUPAIR code to simulate the corresponding increase of yield stress. For the ageing times longer than 2.5 h, the pinning forces of the precipitates were calculated from expression (5). For the 2.5 h ageing time, we used the expression (5) multiplied by

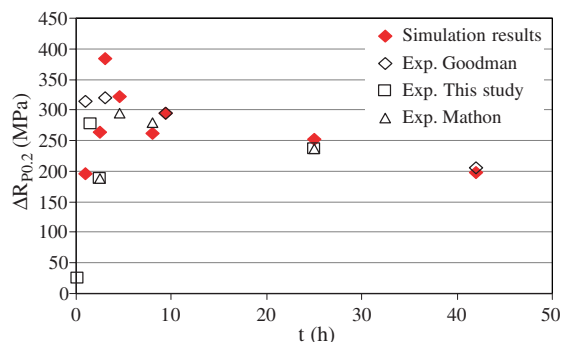


Fig. 16. Simulation of the evolution of the yield stress at 20 °C of Fe–1.5%Cu alloys during ageing at 500 °C. Comparison with experimental results from [61,62].

0.85 to allow for the presence of about 15% of iron in the precipitates (see Section 4.2).

The volume of crystal simulated with DUPAIR was adjusted so that 5000 defects were taken into account in each simulation. For each ageing time, we carried out five simulations with different random distributions of defects and we took into account the softening of the solid solution resulting from the copper depletion. This softening was assessed from (10) and the expressions established by Akamatsu [66]: $\Delta H_v = 32\Delta C_{Cu_{sol}}$, where ΔH_v is the decrease of hardness associated to a decrease $\Delta C_{Cu_{sol}}$ (wt%) of the copper content in solid solution. The average results obtained are plotted in Fig. 16; the agreement with experimental results is good. As aforementioned, this agreement may mean that the temperature dependence of the pinning force observed by Bacon and Osetsyky is lower for screw dislocations than for edge ones.

Vacancy clusters and SIA loops: results published by Eldrup et al. [64] are summarized in Table 9. With the measured sizes and number densities of point defect clusters, DUPAIR simulates an increase of yield stress of 30 and 45 MPa for the doses of 0.009 dpa and 0.23 dpa, respectively. As expected, These values are lower than the measured ones, but have the right order of magnitude.

Table 8
Ageing of Fe–1.5%Cu alloys – mechanical testing and SANS results obtained by Goodman et al. [61] and Mathon [62]

	Ageing time (h)										
	1 ^a	2.5 ^b	3 ^a	4.5 ^b	8 ^b	9.4 ^a	25 ^b	42 ^a	124 ^a	142 ^b	312 ^b
Number density of the Cu precipitates (10^{22} m^{-3})	95	200	100	17	8	11	7	2.8	0.8	0.7	0.4
Mean radius of the Cu precipitates (10^{-9} m)	0.8	0.9	1.2	2.3	2.9	2.8	3	4.8	7.3	6.3	8
Increase of hardness (H_v)	–	75	–	118	112	–	95	–	–	62	53
Increase of yield stress (MPa)	314	–	321	–	–	295	–	205	124	–	–

^a From [61].

^b From [62].

Table 9

Results of tensile tests, TEM experiments and positron annihilation experiments carried out by Eldrup et al. on iron irradiated at 70 °C in HFIR [64]

Dose (dpa)	Vacancy clusters		SIA loops (10^{22} m^{-3})	$\Delta R_{\text{P0.2}}$ at 70 °C	
	Diameter (nm)	Number density (10^{24} m^{-3})		Measured (MPa)	Simulated (MPa)
0.009	0.35	≈ 0.5	1	≈ 80	30
	0.55	≈ 1.7			
	0.75	≈ 0.2			
	1	≈ 0.05			
0.23	0.55	≈ 3.4	5	≈ 180	45
	0.75	≈ 0.7			
	1	≈ 0.08			

6. Conclusion

The interactions between a screw dislocation and irradiation-induced defects in RPV steels were studied from a simplified approach based on static molecular dynamics simulations (the dislocation is immobile and the defect is displaced). The pinning forces exerted by the defects on the dislocations were estimated from the obtained results and some hypotheses. Comparisons with experimental results showed that the proposed values provide a reasonable order of magnitude and can be used as input parameters of a Foreman and Makin-type code to simulate irradiation-induced increase of yield stress of RPV steels. This is the approach that was adopted to build RPV-1. It can be improved in many obvious ways: assessment of the pinning forces with fixed obstacles and gliding dislocations, simulation of the hardening with a dislocation dynamics code, etc.

References

- [1] T. De la Rubia, V.V. Bulatov, MRS Bull. 26 (2001) 169.
- [2] G.R. Odette, B.D. Wirth, D.J. Bacon, N.M. Ghoniem, MRS Bull. 26 (2001) 176.
- [3] S. Jumel, C. Domain, J. Ruste, J.C. van Duysen, C. Becquart, A. Legris, P. Pareige, A. Barbu, E. Van Walle, R. Chaouadi, M. Hou, G.R. Odette, R. Stoller, B.D. Wirth, J. Testing Eval. 30 (2002) 37.
- [4] L. Malerba, E. van Walle, C. Domain, S. Jumel, J.C. van Duysen, Proceedings of ICONE-10: 10th International Conference on Nuclear Engineering, Arlington, USA, 2002.
- [5] S. Jumel, RPV-1: A first virtual reactor to simulate irradiation effects light water reactor pressure vessel steels, PhD thesis, Université de Lille, 2005.
- [6] S. Jumel, J.C. van Duysen, J. Nucl. Mater. 328 (2004) 151.
- [7] S. Jumel, J.C. van Duysen, J. Nucl. Mater. 340 (2005) 125.
- [8] S. Jumel, J.C. Van Duysen, AIEA, submitted for publication.
- [9] G.R. Odette, G.E. Lucas, Radiat. Eff. Def. Solids 144 (1998) 189.
- [10] G.R. Odette, B.D. Wirth, J. Nucl. Mater. 251 (1997) 157.
- [11] P. Pareige, Etude à la Sonde Atomique de l'Evolution Microstructurale sous Irradiation d'Alliages Ferritiques Fe–Cu et d'Aciers de Cuve de Réacteurs Nucléaires, PhD thesis, Université de Rouen, 1994.
- [12] G.R. Odette, G.E. Lucas, ASTM-STP 909 (1986) 206.
- [13] W.J. Phythian, A.J.E. Foreman, C.A. English, J.T. Buswell, M.G. Hetherington, K. Roberts, S. Pizzini, ASTM-STP 1125 (1992) 131.
- [14] K.C. Russell, L.M. Brown, Acta Metall. 20 (1972) 969.
- [15] T. Harry, D.J. Bacon, Acta Mater. 50 (2002) 195.
- [16] X. Li, Etude des Processus de Formation des Microcavités dans les Alliages Ferritiques des Cuves des Réacteurs Nucléaires, PhD thesis, Université Joseph Fourier-Grenoble 1, 1995.
- [17] P. Coulomb, J. Friedel, Dislocations and mechanical properties of crystals, Lake Placid Conference, 1956, Wiley, New York, 1957, p. 555.
- [18] Y.N. Osetsky, D.J. Bacon, Modell. Simul. Mater. Sci. Eng. 11 (2003) 247.
- [19] R. Bullough, R.C. Newman, Philos. Mag. 7 (1962) 529.
- [20] M. Akamatsu, J.C. van Duysen, P. Pareige, P. Auger, J. Nucl. Mater. 225 (1995) 192.
- [21] M.A. Puigvi, Y.N. Osetsky, A. Serra, Philos. Mag. A 83 (2003) 857.
- [22] B.D. Wirth, G.R. Odette, D. Maroudas, G.E. Lucas, J. Nucl. Mater. 276 (2000) 33.
- [23] E. Kuramoto, J. Nucl. Mater. 276 (2000) 143.
- [24] Y. Osetsky, A. Serra, B.N. Singh, S.I. Golubov, Philos. Mag. A 80 (2000) 2131.
- [25] A.E. Ward, S.B. Fisher, J. Nucl. Mater. 166 (1989) 227.
- [26] E.A. Little, R. Bullough, M.H. Wood, Proc. Roy. Soc. Lond. A 372 (1980) 565.
- [27] N. Soneda, T. Diaz de La Rubia, Philos. Mag. A 78 (1998) 995.
- [28] Y.N. Osetsky, D.J. Bacon, A. Serra, B.N. Singh, Golubov, J. Nucl. Mater. 276 (2000) 65.
- [29] J. Marian, B.D. Wirth, J.M. Perlado, Phys. Rev. Lett. 88 (25) (2002) 25507.
- [30] F. Kroupa, Philos. Mag. 7 (1962) 783.
- [31] F. Kroupa, P.B. Hirsch, Discuss. Faraday Soc. 38 (1964) 49.
- [32] M. Makin, Philos. Mag. 10 (106) (1964) 695.
- [33] J.P. Hirth, J. Lothe, Theory of Dislocations, 2nd Ed., 1982.
- [34] M. Rhee, H.M. Zbib, J.P. Hirth, H. Huang, T. de la Rubia, Modell. Simul. Mater. Sci. Eng. 6 (1998) 467.

- [35] G. Saada, J. Washburn, *J. Phys. Soc. Jpn.* 18 (supplement I) (1963) 43.
- [36] J. Friedel, *Dislocations*, Pergamon Press, 1964, p. 454.
- [37] H. Kimura, R. Maddin, *Lattice Defects in Quenched Metals*, Academic Press, New York, 1969, p. 319.
- [38] A.J.E. Foreman, J.V. Sharp, *Philos. Mag.* 19 (1969) 931.
- [39] P.B. Hirsch, in: R.E. Smallman, J.E. Harris (Eds.), *Vacancies* 76, 1976.
- [40] B.L. Eyre, A.F. Barrlett, *ibid* 11 (1965) 53.
- [41] D.J. Bacon, Yu.N. Osetsky, *J. Nucl. Mater.* 329–333 (2004) 1233.
- [42] M.T. Kirk, M.A.E. Natishan, M. Wagenhofer, *ASTM-STP-1406*, 2001.
- [43] Y. Aono, E. Kuramoto, K. Kitajima, Report of Research Inst. for Applied Mechanics, vol. 29, Kyushu University, 1981, p. 127.
- [44] D. Farkas, P.L. Rodriguez, *Scr. Metall. Mater.* 30 (7) (1994) 921.
- [45] J. Marian, W. Cai, V. Bulatov, *Nature Mater.* 3 (2004) 158.
- [46] A.J.E. Foreman, M.J. Makin, *Philos. Mag.* 14 (1964) 911.
- [47] C. Domain, S. Jumel, J.C. van Duysen, submitted for publication.
- [48] L.M. Brown, R.K. Ham, in: A. Kelly, R.B. Nicholson (Eds.), *Strengthening Methods in Crystals*, Applied Science, London, 1971, p. 9, Chapter 2.
- [49] A.J.E. Foreman, M.J. Makin, *Can. J. Phys.* 45 (1967) 281.
- [50] D.J. Bacon, U.F. Kocks, R.O. Scattergood, *Philos. Mag.* 28 (1973) 1241.
- [51] V. Shasstry, T. Diaz de la Rubia, *J. Eng. Mater. Technol.* 121 (1999) 126.
- [52] C.S. Becquart, K.M. Decker, C. Domain, J. Ruste, Y. Souffez, J.C. Turbatte, J.C. Van Duysen, *Radiat. Eff. Def. Solids* 142 (1997) 9.
- [53] M. Ludwig, D. Farkas, D. Pedraza, S. Schmauder, *Model. Simul. Mater. Sci. Eng.* 6 (1998) 19.
- [54] H. Suzuki, A.R. Rosenfield, G.T. Hahn, A.L. Bement, R.I. Jaffee (Eds.), *Dislocation Dynamics*, McGraw-Hill, 1968, p. 679.
- [55] V. Vitek, *Cryst. Lattice Defects* 5 (1974) 1.
- [56] V. Vitek, R.C. Perrin, D.K. Bowen, *Philos. Mag.* 21 (1970) 1049.
- [57] A.H. Cottrell, *Dislocations and Plastic Flow in Crystals*, Oxford, 1953.
- [58] A.J.E. Foreman, *Acta Metall.* 3 (1955) 322.
- [59] Domain, private communication.
- [60] P.J. Othen, M.L. Jenkins, G.D.W. Smith, W.J. Phythian, *Philos. Mag. Lett.* 64 (1991) 383.
- [61] S.R. Goodman, S.S. Brenner, J.R. Low, *Metall. Trans.* 4 (1973) 2363.
- [62] M.H. Mathon, Etude de la précipitation et des mécanismes microscopiques de durcissement sous irradiation dans des alliages ferritiques dilués, Thèse de doctorat, Université Paris Sud, Orsay, 1995.
- [63] Private communication.
- [64] M. Eldrup, B.N. Singh, S.J. Zinkle, T.S. Byun, K. Farrell, *J. Nucl. Mater.* 307–311 (2002) 912.
- [65] J. Marian, B.D. Wirth, R. Schaublin, G.R. Odette, J.M. Perlado, *J. Nucl. Mater.* 323 (2003) 181.
- [66] M. Akamatsu-Jousset, Evolution microstructurale d'alliages ferritiques sous irradiation, Thèse de Doctorat, Université Paris-Sud, Orsay, 1994.